SUPPORTING INFO

Enhanced catalytic activity of nanostructured, A-site deficient $(La_{0.7}Sr_{0.3})_{0.95}(Co_{0.2}Fe_{0.8})O_{3-\delta}$ for SOFC cathodes

Ozden Celikbilek[a,b*], Cam-Anh Thieu[c,d], Fabio Agnese[e], Eleonora Cali[b], Christian Lenser[f], Norbert H. Menzler[f], Ji-Won Son[c,d], Stephen J. Skinner[b], Elisabeth Djurado[a]

a. Univ. Grenoble Alpes, Univ. Savoie Mont Blanc, CNRS, Grenoble INP, LEPMI, 38000, Grenoble, France
b. Department of Materials, Imperial College London, Prince Consort Road, London SW7 2BP, United Kingdom
c. Center for Energy Materials Research, Korea Institute of Science and Technology (KIST), Hawolgok-dong, Seongbuk-gu, Seoul 02792, Korea
d. Division of Nano & Information Technology, KIST School, Korea University of Science and Technology (UST), Hawolgok-dong, Seongbuk-gu, Seoul 02792, Korea
e. Univ. Grenoble Alpes, INAC-SyMMES, F-38054 Grenoble Cedex 9, France.
f. Forschungszentrum Jülich GmbH, Institute of Energy and Climate Research: Materials Synthesis and Processing (IEK-1), 52425 Jülich, Germany

*Corresponding author: o.celikbilek@imperial.ac.uk

a) Elemental Analysis

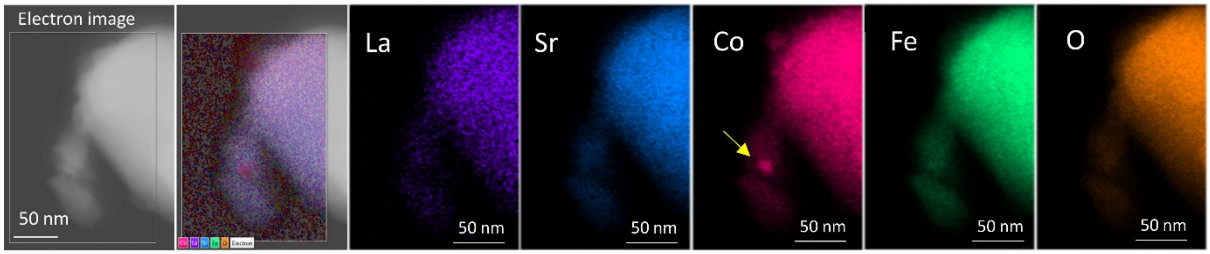

Fig. S. 1 STEM ADF-EDX maps of LSCF particles removed from the sintered film.

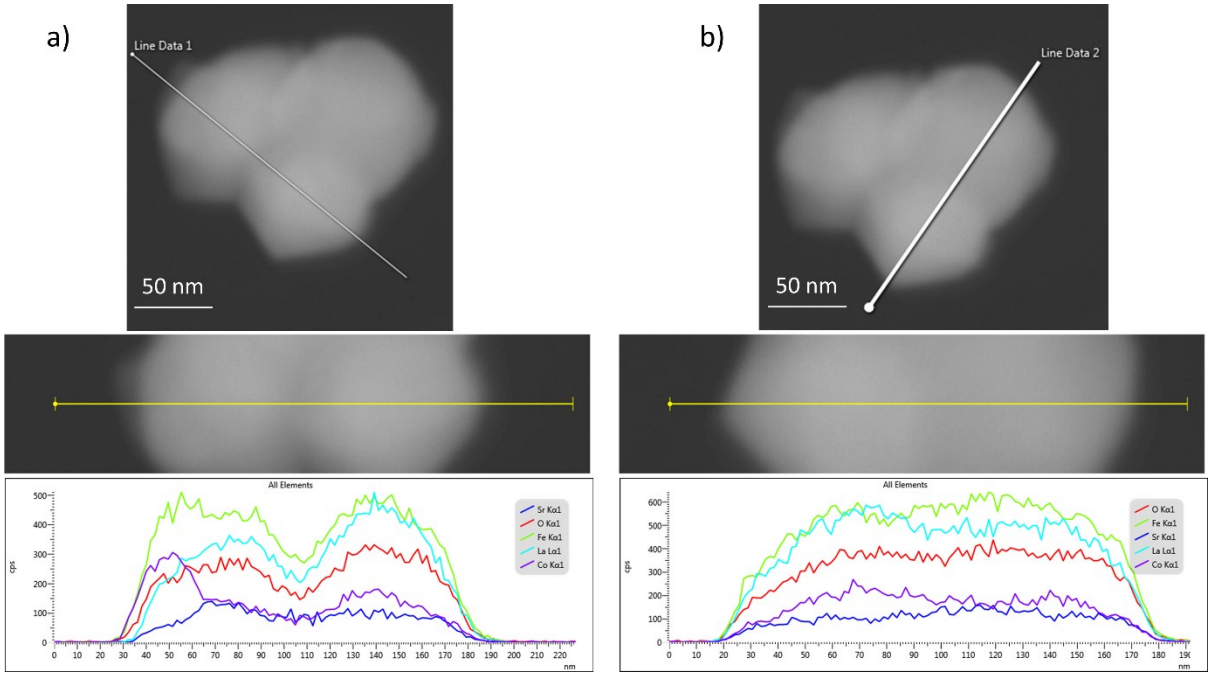

Fig. S. 2 STEM ADF-EDX line scans across LSCF particles removed from the sintered film.

b) Electrochemical Impedance Spectroscopy Analysis

Fig. S. 3 shows the impedance spectra (650-450 °C) and corresponding equivalent circuit fitting of ESD films (550-450 °C).

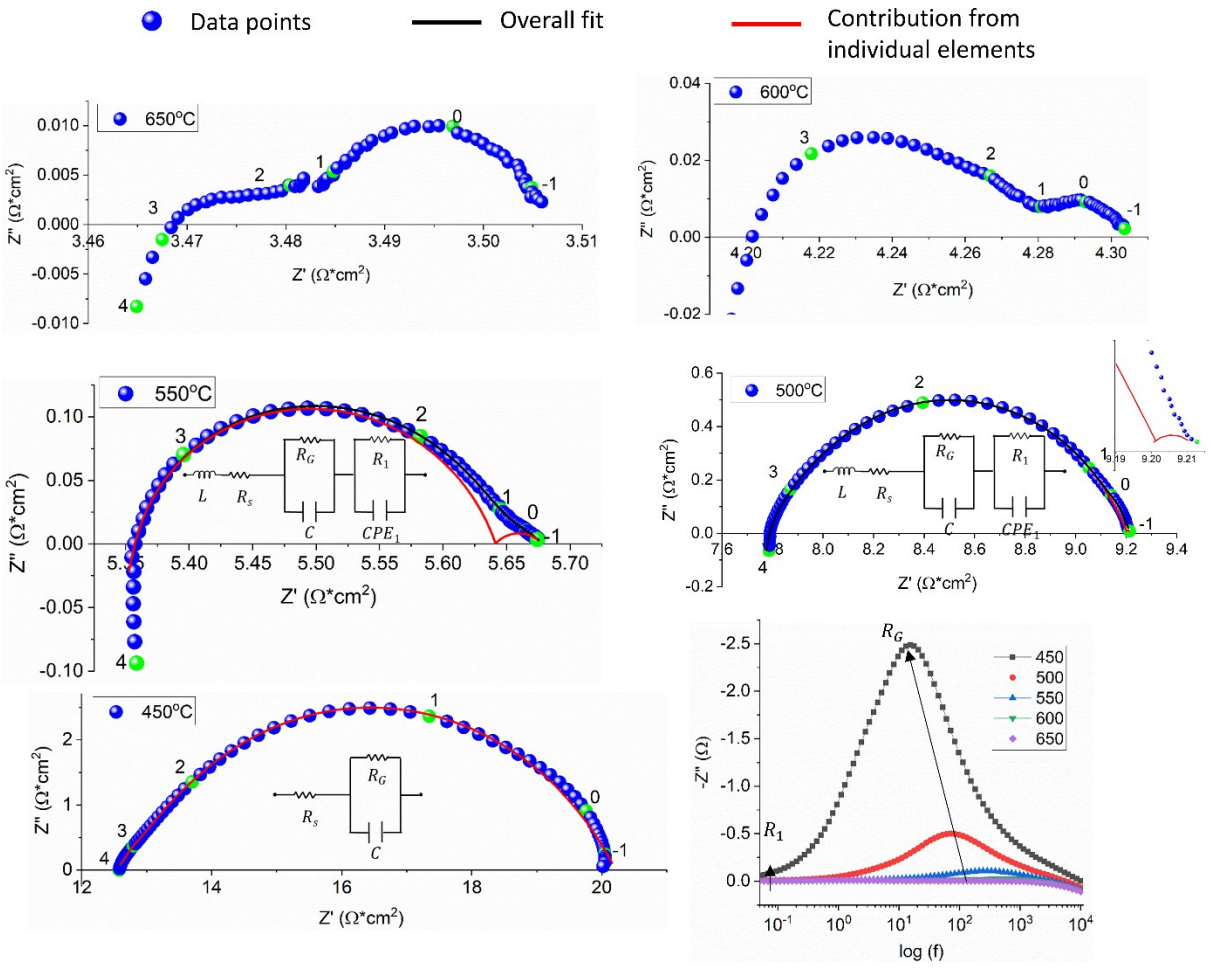

Fig. S. 3 Nyquist and Bode plots of LSCF ESD films measured in air and OCV conditions at 650-450 °C. The green points on the Nyquist plots are frequency values in the logarithmic scale. The spectra at 550-450 °C were fitted with R_s-R_G//C circuit, R_1//CPE_1 element has been added in series at ≥ 500 °C. L represents inductance of the wires; R_s series resistance of the electrolyte; R_G Gerischer impedance; R_1 connected in parallel to a constant phase element CPE_1 represent bulk diffusion of oxygen in the gas layer.

Equivalent circuit fitting was performed only on the data recorded at lower temperatures (450 and 550 °C). A Gerischer impedance, $Z(\omega)$ in (Eq.1), corresponds to a co-limited situation of diffusion and surface exchange in porous mixed ionic-electronic oxides.[1]

$$Z(\omega) = \frac{R_g}{\sqrt{1 + (j\omega t_g)^n}} \quad \text{(Eq. S1)}$$

where ω is the angular frequency, R_g and t_g are the characteristic resistance and time constant, respectively. First, t_g is calculated using the formula $t_g \cdot \omega_{max} = \sqrt{3}/2\pi$ where ω_{max} is the summit frequency of the Gerischer impedance. In the case of a non-ideal form of the impedance, an n- parameter is introduced.[2] The n-value used in this work is between 0.8 and 0.9. The oxygen surface exchange coefficient, k_o (cm s^{-1}), and bulk diffusion coefficient D_o (cm^2 s^{-1}) are then calculated from the Gerischer impedance at all temperatures according to:

$$k_o = \frac{c_v(1-\varepsilon)\,1}{c_o\ a\ \gamma\ \ t_g} \qquad \text{(Eq. S2)}$$

$$D_o = \left(\frac{RT}{4F^2}\right)^2\left(\frac{\tau}{(1-\varepsilon)aR_g^2k_oC_o^2}\right) \qquad \text{(Eq. S3)}$$

where ε, a, and τ are microstructure-related parameters, which are porosity, specific surface area (cm^{-1}) and tortuosity, respectively. R is the ideal gas constant (J K^{-1} mol^{-1}), F the Faraday's constant (C mol^{-1}) and T the temperature (K). γ is the thermodynamic factor which relates the differential changes in oxygen partial pressure to the oxygen stoichiometry of the perovskite. Finally, c_o and c_v are the oxygen equilibrium concentration and oxygen ion lattice site concentrations (mol cm^{-3}), respectively. The summit frequency of the Gerischer contribution shifts from ~20 Hz at 450 °C to approximately 40 Hz at 650 °C. As the fitting at $\geq$ 600 °C could not be performed, the oxygen surface exchange and bulk diffusion values in these points were estimated by following the frequency trend of the Gerischer impedance in the Bode plot. All microstructure- and thermodynamic- related values can be found in ref. [3]. The oxygen transport parameters (D_o, k_o) calculated from the Gerischer impedance spectra are related to those measured by isotopic tracer experiments (D^*, k^*). The following equation holds for the transformation: $D^* = D_o \cdot f_o$ where f_o is the correlation factor for tracer diffusion and is equal to 0.67 for the perovskite lattice.[4] For the surface exchange, $k^* \cong k_o$ is assumed.[5] The chemical transport parameters (D_{chem}, k_{chem}) measured by conductivity and gravimetric relaxation techniques are related to (D_o, k_o) via the thermodynamic enhancement factor, γ: $D_{chem} = D_o\frac{c_o}{c_v}\gamma$ and $k_{chem} = k_o\frac{c_o}{c_v}\gamma$.

For the microstructural parameters, we have previously shown that the following equation holds for LSCF films deposited by the ESD technique sintered at 800 °C for 2h assuming cylindrical interconnected pores.[3]

$$a = \frac{2 \times \varepsilon}{r} \qquad \text{(Eq. S4)}$$

The specific surface area (a) is computed as a function of porosity (ε) and pore radius (r). The pore radius of LSCF films in this work (sintered at 900 °C for 2h) is approximately 100 nm. Therefore, variable microstructural parameters were used to estimate the ASR of LSCF films in this work: ε =10-50 %, a = 2-10 μm^{-1} was assumed. τ factor was also varied between 1-10. Oxygen self-diffusion (D_o) and surface exchange coefficients (k_o) were taken from Benson *et al*. as 2.19×10^{-10} $cm^2\ s^{-1}$ and 3.37×10^{-7} $cm\ s^{-1}$. [6]

c) Catalytic Effect of CFO nanoparticles

New experiments were designed with the nominally stoichiometric $La_{0.6}Sr_{0.4}Co_{0.2}Fe_{0.8}O_{3-\delta}$ cathodes (Sigma-Aldrich, 10-14 m^2/g) to isolate the catalytic effect of the CFO particles. An ink of stoichiometric LSCF 6428 powder was screen-printed onto GDC substrates and subsequently sintered at 950 °C for 2h in air. In order to mimic the small particle size of the CFO particles, 0.6 M and 6 µL CFO solution (50/50 ethanol: deionised water) was infiltrated into the LSCF backbone to obtain particles at the nanometre length scale. The sample was dried at 350 °C for 30 min and was measured in the impedance from 450 °C to 750 °C on heating and cooling, respectively. The temperature during impedance measurements was increased to 750 °C to increase the CFO particle size, similar to ESD film. The loading of the CFO was verified by measuring the weight change of the sample before and after the infiltration.The loading was chosen as ~4 wt. %, also similar to the ESD films (~6 wt. %). The XRD diffractograms were taken on the bare LSCF samples deposited on the GDC and the CFO

infiltrated samples after the impedance measurements (Fig. S. 4). The diffraction peaks corresponding to the CFO phase were observed in the infiltrated film while the bare film had no additional peaks.

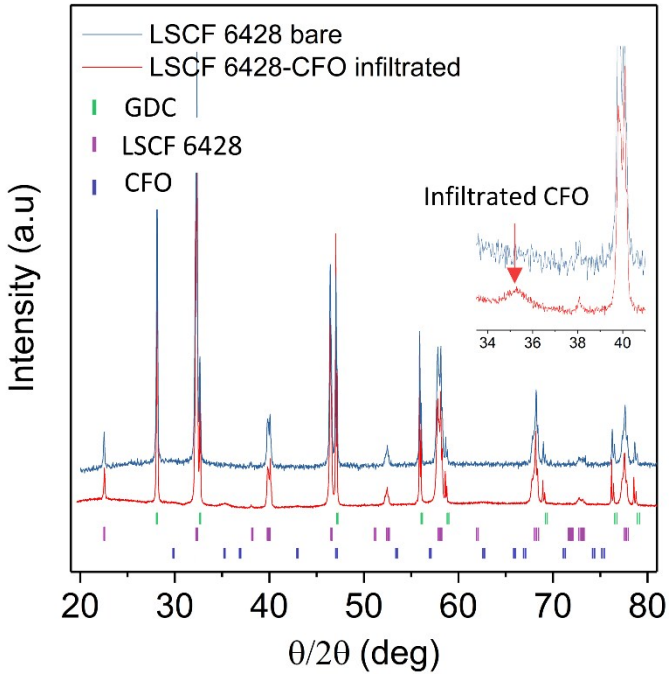

Fig. S. 4 XRD diffractograms of bare LSCF 6428 film and with CFO infiltration.

The impedance spectra at 450 and 750 °C (Fig. S. 5 a-d) were deconvoluted into different semicircles in the complex impedance plane plots. At each temperature, a corresponding equivalent circuit was proposed, and the identified loss mechanisms were assigned to electrochemical processes. An inductance L, a series resistance R_s and a fractal Gerischer impedance R_G representing co-limited bulk diffusion and surface exchange reactions at the cathode. An additional R//CPE element (a resistor in parallel with a constant phase element) was added before the Gerischer element at low-temperatures (450 °C), which was assigned to charge transfer resistance at the electrode/electrolyte interface. Fig. S. 6 shows the Arrhenius plot of area specific resistance of the Gerischer impedance (R_G) of the bare and the infiltrated LSCF film. It shows a substantial decrease in both the resistance and the activation energy in the infiltrated films.

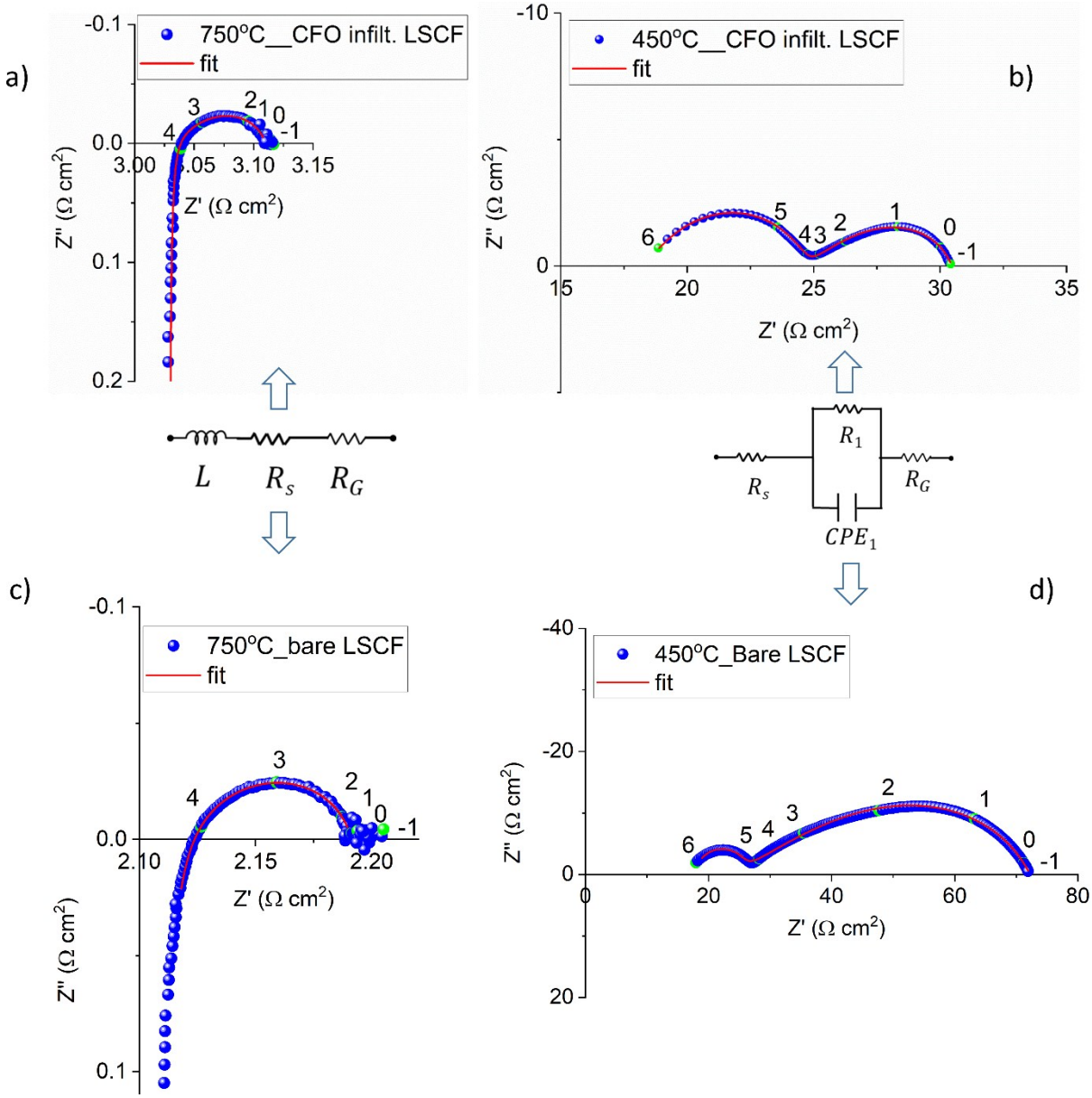

Fig. S. 5 Nyquist plots and corresponding equivalent circuit fits of the CFO infiltrated LSCF and the bare LSCF films measured in air and OCV conditions. The impedance spectra of the CFO infiltrated film plotted on heating up at a) 750 and b) 450 °C a); and the bare stoichiometric LSCF 6428 films plotted at c) 750 and d) 450 °C. The green points are the frequency values in the logarithmic scale. The inset drawings show the equivalent circuit models used in the fitting. L represents inductance of the wires; R_s series resistance of the electrolyte; R_G fractal Gerischer impedance, the n-value used in this work was ~0.75; R_1 connected in parallel to a constant phase element CPE_1 represent charge transfer reactions at the cathode/electrolyte interface.

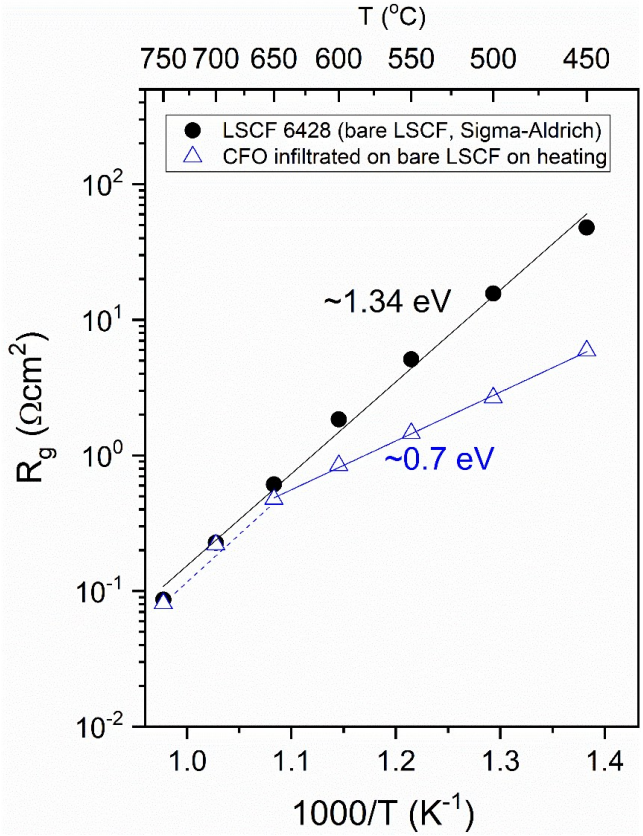

Fig. S. 6 Arrhenius plot of the Gerischer resistance normalised by the cathode area (R_g, Ωcm^2) of the bare and the infiltrated LSCF 6428. The impedance spectra of the infiltrated film have been analysed on heating. Activation energy (E_a) of the infiltrated film has been calculated only between 450-650 °C. There is a clear change in E_a above 650 °C, which is attibuted to the rapid agglomeration of CFO particles.

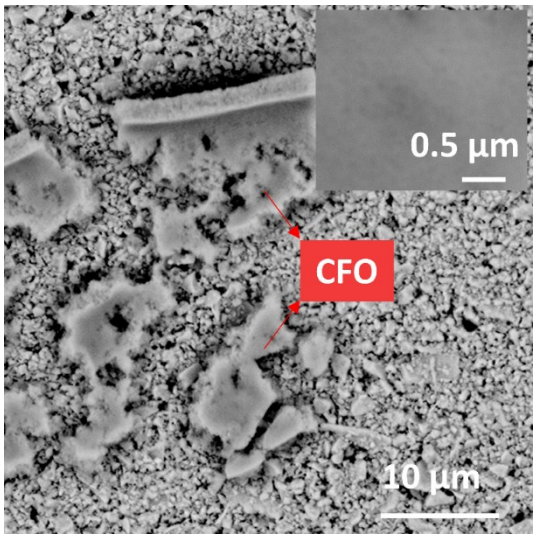

Fig. S. 7 SEM images of stoichiometric LSCF 6428 as a functional layer and CFO infiltrates after impedance measurements showing agglomeration of CFO particles. Particle coarsening was not observed after impedance measurements (inset image).

d) Single, anode-supported cell test: Electrochemical Impedance Spectra analysis by Complex Nonlinear Least Square (CNLS) Fitting Algorithm

CNLS fitting: the equivalent circuit (EC) model is based on the model developed by Leonide et al. for anode-supported SOFC made in Jülich.[7]

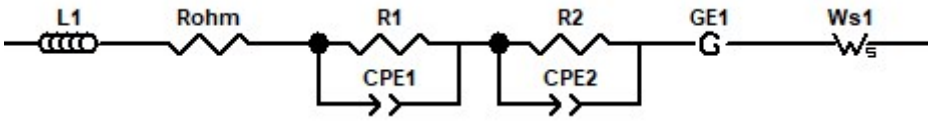

Fig. S. 8: Equivalent circuit model used to fit the impedance of SOFC full cells

L1 describes the inductance in the test setup, R_{ohm} the ohmic resistance (electrolyte + contact resistance), R_1/CPE_1 and R_2/CPE_2 describe processes related to the anode, GE_1 describes the oxygen reduction reaction in the cathode, and Ws_1 describes the gas diffusion polarization in the support. Since the EC elements representing the anode are not clearly associated to physico-chemical processes in the anode [8], both EC elements together are simply taken as the total anode impedance.

The main modification to the equivalent circuit developed by Leonide et al.[7] is that a circuit element for gas diffusion impedance in the cathode (which is not measurable in air) is not included. The Warburg element Ws_1 describing gas diffusion in the anode support is only included for the spectra recorded at 650 °C and 600 °C at the lowest cell voltage (highest current). It typically yields a gas-diffusion resistance of about 30 mΩ cm², and is generally relevant only at elevated temperatures (when other cell impedances are small) or at high fuel utilization (e.g. in an SOFC stack or at high current density). This is visible in the anode impedance at 550 mV, where divergence from Arrhenius behaviour can be seen for 600 °C and 650 °C. Under OCV conditions and at 750 mV cell voltage, the contribution of Ws_1 is not discernible in the impedance spectrum.

The following graphs (Fig. S. 9 and Fig. S. 10) is for the data recorded at 600 °C and a cell voltage of 750 mV. They are representative for the fitting procedure of all data shown for the full cell tests: first, the data was checked for quality using the Lin-KK software tool.[9–11]

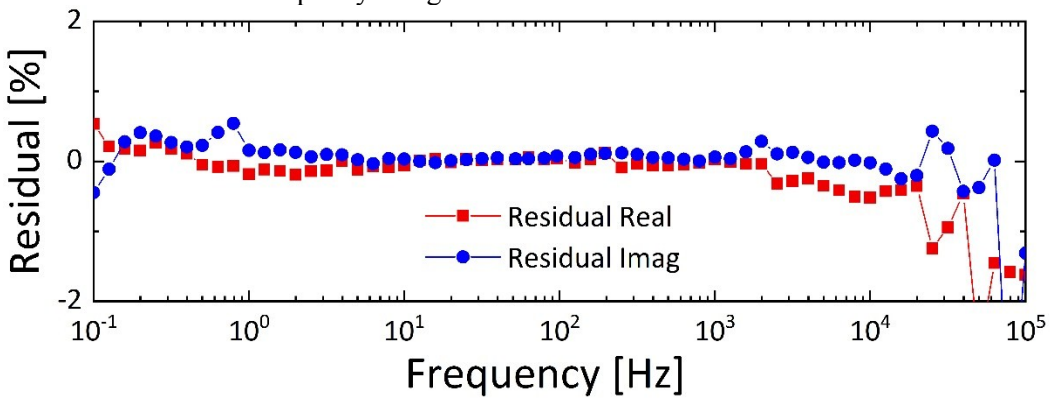

Fig. S. 9: Residuals of the linear Kramers-Kronig transformation of the raw data.

Subsequently, impedance data were fitted using the EC model shown in Fig. S. 8. The fit of the impedance spectrum is shown in Fig. S. 10 a), and the residuals in b).

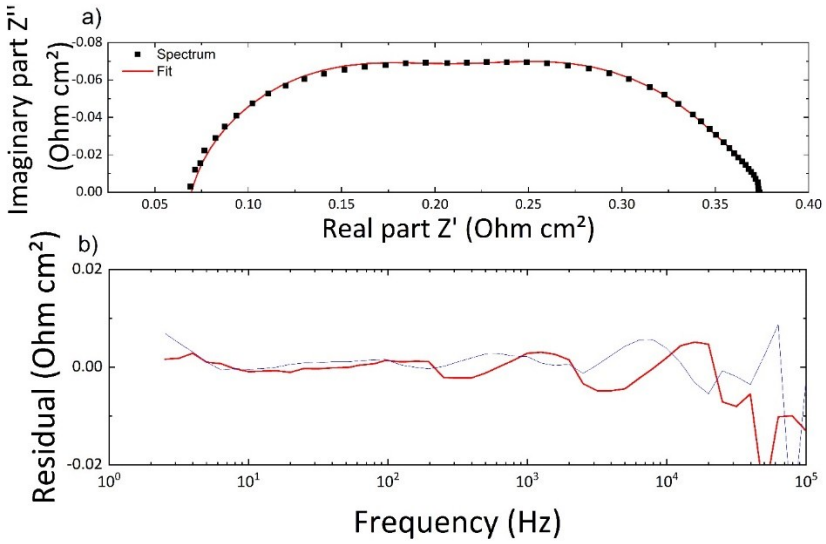

Fig. S. 10 a): Impedance data (black squares) and CNLS fit (red line) of the data recorded at 600 °C and 750 mV. b) Residuals vs frequency of the fit shown in a).

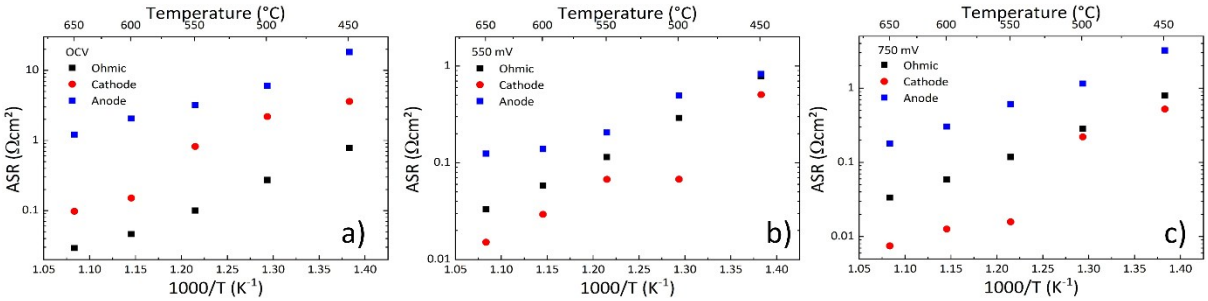

Fig. S. 11 Complex Nonlinear Least Square (*CNLS*) fitting[7] of impedance data of anode-supported cells in a) OCV, b) 550 mV and c) 750 mV.

References

1 S. Adler, *Solid State Ionics*, 1998, **111**, 125–134.
2 B. A. Boukamp and H. J. M. Bouwmeester, *Solid State Ionics*, 2003, **157**, 29–33.
3 O. Celikbilek, D. Jauffrès, E. Siebert, L. Dessemond, M. Burriel, C. L. Martin and E. Djurado, *J. Power Sources*, 2016, **333**, 72–82.
4 T. Ishigaki, S. Yamauchi, K. Kishio, J. Mizusaki and K. Fueki, *J. Solid State Chem.*, 1988, **73**, 179–187.
5 S.-N. Lee, A. Atkinson and J. A. Kilner, *J. Electrochem. Soc.*, 2013, **160**, F629–F635.
6 S. Benson, *PhD Thesis*, Dept. Mater., 1999, Imperial College London.
7 A. Leonide, V. Sonn, A. Weber and E. Ivers-Tiffée, *J. Electrochem. Soc.*, 2008, **155**, B36–B41.
8 S. Dierickx, T. Mundloch, A. Weber and E. Ivers-Tiffée, *J. Power Sources*, 2019, **415**, 69–82.
9 B. A. Boukamp, *J. Electrochem. Soc.*, 1995, **142**, 1885–1901.
10 M. Schönleber, D. Klotz and E. Ivers-Tiffée, *Electrochim. Acta*, 2014, **131**, 20–27.
11 M. Schönleber and E. Ivers-Tiffée, *Electrochem. commun.*, 2015, **58**, 15–19.